Conference paper

Roman Bulánek* and Pavel Čičmanec

Textural and morphology changes of mesoporous SBA-15 silica due to introduction of guest phase

DOI 10.1515/pac-2016-1017

Abstract: The research focuses on study of guest phase effect on the surface area and pore volume of SBA-15 with the emphasis on elucidation of reasons for these changes. The changes of surface area and pore volume are evident from evaluated N_2 adsorption isotherms of VOx-SBA-15 even for samples with relative low content of supported guest phase, which is "atomically" spread on the surface in the form of anchored monomeric vanadyl species. These species cannot block the pore with diameter of 10 nm, nevertheless the presence of such phase causes decrease in adsorbed nitrogen during physisorption. Comparison of guest phase amount with differences in adsorbed amount of nitrogen led to conclusion that each vanadyl complex prevents adsorption of about one or two N_2 molecules in the layer and influences two adsorption layers. Significant pore blocking occurs in the VOx-SBA-15 materials only in the case of presence bulk oxide-like nanospecies. Re-structuralization of silica mimicking phase separation phenomena relying on spinodal decomposition of a system was observed by SEM/TEM analysis and adsorption isotherms inspection for materials with high vanadium content.

Keywords: adsorption; SBA-15; SSC-2016; surface area; texture; vanadium.

Introduction

Ordered mesoporous silicas, with uniform pore size distribution and high surface area, are interesting materials for a wide variety of applications, such as catalyst supports [1–3], adsorbents [4], and drug delivery system [5]. One of the most frequently applied and investigated mesoporous silica is SBA-15 material. SBA-15 is a mesoporous silica sieve with the uniform hexagonal pores with the narrow pore size distribution and tunable pore diameter having thicker framework walls, which increases hydrothermal and mechanical stability of the material. Hexagonal SBA-15 silica has been tested for many applications in the field of catalysis, usually as a support of active phase. It is very often reported in the literature [6–26] that the introduction of even small amount of guest phase into mesoporous supports can greatly affect their textural properties, determined mostly by evaluation of N_2 adsorption isotherms data. Observed changes in surface area and other texture parameters were very often attributed to a partial destruction/modification of the framework [7, 10–12], pore blocking [8, 13–18], or changing roughness of the surface [19–22]. These explanations of the observed changes are full of contradictions in some cases, especially in the cases of guest complexes which are much

Article note: A collection of invited papers based on presentations at the 12th Conference on Solid State Chemistry (SSC-2016), Prague, Czech Republic, 18–23 September 2016.

***Corresponding author: Roman Bulánek,** Department of Physical Chemistry, Faculty of Chemical Technology, University of Pardubice, Studentská 573, 532 10 Pardubice, Czech Republic, e-mail: roman.bulanek@upce.cz
Pavel Čičmanec: Department of Physical Chemistry, Faculty of Chemical Technology, University of Pardubice, Studentská 573, 532 10 Pardubice, Czech Republic

smaller than pores size (in the case well-dispersed metal-oxo complexes that are more than ten times smaller compared with pore size) and when total amount of guest phase is only few wt. %. Even in such cases, the decrease in surface area and pore volume reached frequently large extent often exceeding 20–50 rel. %.

To the best of our knowledge there are no reports on systematic study of guest phase effect on the surface area and pore volume of SBA-15 with the emphasis on elucidation of reasons for these changes. We report detailed study of textural properties of VOx-SBA-15 mesoporous silica catalysts and their variation depending on vanadium content and population of individual VOx complexes. System of VOx-SBA-15 catalysts was chosen due to importance of supported vanadium oxide catalysts in variety of selective oxidation reactions [27–29]. In the following we will show that the presence of even isolated vanadyl (VO_4) species on the surface excludes some volume and surface of the pore from the adsorption, which leads to lowering the monolayer adsorption capacity and thus formally to reduce the surface area even when the structure and the surface of the support has not changed. In addition, re-structuralization of the silica mimicking Cahn-Hilliard phase separation phenomena [30] relying on spinodal decomposition of a sol-gel system was observed by SEM/TEM analysis and hysteresis loop of capillary condensation inspection for catalysts with high vanadium content.

Experimental

Purely siliceous SBA-15 mesoporous molecular sieve was synthesized according to procedure described elsewhere [31]. Vanadium oxo-complexes were anchored onto SBA-15 silica surface by standard wet impregnation procedure by appropriate amount of ethanol solution of vanadyl acetylacetonate (Aldrich) described in our previous papers [29, 32]. Samples are denoted by following manner: x-SBA-15, where x stands for vanadium content in the wt. % followed by abbreviation of silica structure (SBA-15).

The vanadium content was determined by means of ED XRF by ElvaX (Elvatech, Ukraine) equipped with Pd anode. Samples were measured against the model samples (a mechanical mixture pure SiO_2 and $NaVO_3$) granulated to the same size as catalysts. Vanadium contents in individual samples are reported in the Table 1.

The crystallographic structure of the catalysts was determined by examining the X-ray diffraction (XRD) patterns of the powder samples obtained by using a D8 Advance Eco (Bruker AXS) applying CuKα radiation ($\lambda = 1.5406$ Å). The step size of 0.02° and a step time of 0.5 s were used. The patterns were collected over the 2θ range from 0.5° to 10° and from 10° to 70° and evaluated by using the Diffrac.Eva V 4.1.1.

Table 1: Structural characteristics of VOx-SBA-15 materials.

Sample code	w_v wt. %	C	S_{BET} $m^2\,g^{-1}$	V_p $cm^3\,g^{-1}$	d_p nm	a_0 nm	$(\Delta n_{monolayer})/n_v$
SBA-15	–	101.4	762 ± 2.0	0.971	10.4	11.03	–
1-SBA-15	1.13	98.0	736 ± 1.8	0.948	10.4	11.19	0.94
2-SBA-15	1.97	101.4	713 ± 1.7	0.923	10.4	11.14	0.88
3-SBA-15	3.01	101.6	680 ± 1.4	0.898	10.3	11.05	1.03
4-SBA-15	4.04	103.6	633 ± 1.3	0.859	10.3	11.11	1.28
5-SBA-15	5.01	102.2	602 ± 1.1	0.827	10.2	11.09	1.27
6-SBA-15	6.04	98.3	566 ± 1.0	0.780	10.1	11.01	1.31
7-SBA-15	6.99	110.7	489 ± 1.0	0.694	10.0	10.92	1.63
8-SBA-15	7.80	105.8	493 ± 0.8	0.717	10.1	10.94	1.36
9-SBA-15	8.97	107.1	421 ± 0.7	0.634	10.1	10.84	1.58
12-SBA-15	11.98	99.9	318 ± 0.4	0.459	10.0	10.88	1.53
20-SBA-15	20.08	120.5	87 ± 0.2	0.012	–	–	1.36

w_v, mass fraction of vanadium; C, interaction constant in BET equation; S_{BET}, BET specific surface area; V_p, total pore volume; d_p, pore diameter calculated by NL DFT approach; a_0, lattice spacing; $(\Delta n_{monolayer})/n_v$, average number of "missing" nitrogen molecule in monolayer per vanadium atom.

Morphology of the catalysts was investigated by means of SEM and TEM images. SEM images of VOx-SBA-15 materials were acquired by means of JEOL JSM 7500F scanning electron microscope with a cold cathode – field emission (parameters of measurements: 1 kV, GB high mode). Transmission electron microscopy (TEM) was carried out on a JEOL JEM 3010 microscope operated at 300 kV (LaB_6 cathode, point resolution 1.7 Å). Images were recorded on a CCD camera with resolution 1024 × 1024 pixels using the Digital Micrograph software package.

Specific surface area and pore volume of investigated samples were measured by means of nitrogen adsorption/desorption at temperature of liquid nitrogen (77.2 K) by using ASAP 2020 equipment (Micromeritics, USA). Prior to adsorption isotherm measurement, the samples were degassed by slow heating (2 °C/min) to 250 °C and maintaining this temperature for 8 h under turbomolecular pump vacuum. The specific surface area was calculated according to BET method [33, 34]. The BET surface area was evaluated by using adsorption data in the relative nitrogen pressure range $x > 0.05$ until the slope of the so called Rouquerol's plot *ie.* $n_{ads} \cdot (1 - x)$ *vs* x is positive [35]. The mesopore size distribution and volume were determined by NL DFT method by using of "N2 @ 77K" model for cylindrical pores and oxide surface [36].

In order to gain information on speciation of vanadium species on the silica surface, diffuse-reflectance UV-vis spectroscopy and Raman spectroscopy were used. The UV-vis diffuse reflectance spectra of diluted and subsequently dehydrated samples were measured using Cintra 303 spectrometer (GBC Scientific Equipment, Australia) equipped with a Spectralon-coated integrating sphere using a Spectralon coated discs as a standard. All Raman spectra were measured under dehydrated conditions. The dehydration and oxidation protocol was the same as for DR UV-vis spectra measurement. The Raman spectra were measured in glass cuvette by Nicolet DXR Smart Raman spectrometer equipped with CCD detection. Spectra were excited by Smart Excitation Laser (Thermo Scientific) with laser wavelength at 780 nm. More details about measurement of DR UV-vis spectra and Raman spectra and their evaluation can be found in the Refs. [37, 38].

Results

In order to investigate changes in textural properties of SBA-15 upon introduction of guest phase (vanadyl complexes), wide set of SBA-15 samples with vanadium content exceeding the concentration range of commonly studied systems (range of vanadium content from 1 wt.% to 20 wt.%) was prepared by wet impregnation of vanadyl acetylacetonate ethanolic solution into pure siliceous SBA-15 support and characterized in detail by XRD, SEM/TEM imaging, N_2 physisorption and DR UV-vis and Raman spectroscopies.

Low-angle diffraction patterns of all investigated samples are shown in the Fig. 1A. All patterns, with only one exception of 20-SBA-15 sample, are similar to each other and exhibit three well resolved peaks that can be indexed on a 2D-hexagonal lattice, and thus, materials can be regarded as SBA-15 silicas. Diffraction peaks can be assigned to (100), (110) and (200) reflections. It is obviously observed that the patterns of the samples showed a decrease in peak intensity with increasing vanadium loading, but maintained *d* spacing ratio between (100), (110) and (200) diffractions proves preservation of hexagonal arrangement. Intensity decrease is probably caused by differences in the scattering contrasts of the pores and walls of silica and formed VOx species inside the pores of SBA-15 [39, 40] or dilution of the silica matrix with increased incorporation of vanadium as results of higher absorption factor of vanadium for X-rays than silicon [41]. A small shift of the diffraction peaks to higher 2θ values relative to the parent SBA-15 material is identified for VOx-SBA-15, possibly due to a small structural shrinkage caused by interaction of silica wall with vanadyl complexes. Lattice constants a_0 for hexagonal lattice, calculated from (200) interplanar distances by means of equation (1), are summarized in the Table 1. The change in a_0 is less than 0.35 nm for all VOx-SBA-15 samples.

$$a_0 = 4\, d_{200} / \sqrt{3} \tag{1}$$

The most loaded sample (20-SBA-15) exhibit no diffraction patterns in the low-angle region, caused by collapse of the regular mesoporous structure, as is proved by SEM and TEM images described later (see Fig. 2).

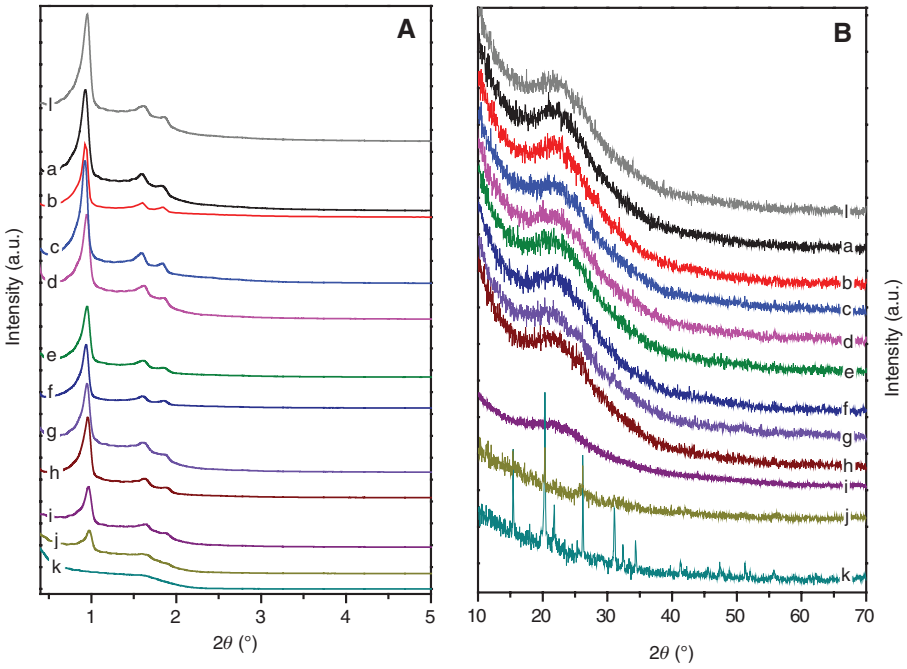

Fig. 1: Powder XRD patterns for VOx-SBA-15 materials in the range of small angles (A) and wide angles (B). a: 1-SBA15, b: 2-SBA15, c: 3-SBA15, d: 4-SBA15, e: 5-SBA15, f: 6-SBA15, g: 7-SBA15, h: 8-SBA15, i: 9-SBA15, j: 12-SBA15, k: 20-SBA15, l: parent SBA15.

On the other hand, wide-angle XRD patterns of SBA-15 samples with vanadium content lower than 12 wt. % are very poor and only broad peak ranging from $2\theta = 15°$ to 30° assigned to amorphous silica wall of the SBA-15 support is visible. 12-SBA-15 and 20-SBA-15 samples exhibit set of diffraction lines at $2\theta = 15.45°$, 20.38°, 21.78°, 26.18°, 31.11°, 32.39°, 34.36°, 41.31°, and 47.44°, which can be ascribed to the crystalline V_2O_5 oxide particles. Presence of larger V_2O_5 crystallites is also proved by SEM images (Fig. 2).

SEM and TEM images of the selected SBA-15 samples are shown in the Fig. 2. Particles of the parent SBA-15 support have a lenticular character of approximately micrometer in size with roughly hexagonal base. The thickness of the particles is about 150 nm at outside edge and significantly more in the center of the particle. The channels are directed across the particle perpendicular to the plane of the base. Regular hexagonal arrangement of parallel cylindrical channels is clearly evident from the images (see Fig. 2A and B). SEM and TEM images of 1-SBA-15 and 9-SBA-15 samples (Fig. 2C–F) confirm that structure and morphology of the particles remain the same as for parent SBA-15. Both samples have well-ordered porosity without visible distortions or collapse. Completely different conclusion can be drawn from micrographs taken on samples with highest vanadium content. In the case of 12-SBA-15 sample, small thin needles of vanadium pentoxide can be observed, which correspond with low-intense diffraction lines in wide-angle XRD pattern of the sample (see. Fig. 1B). Much more significant change concerns of porosity of the SBA-15 particles. Some particles remain rather unchanged, but large part of particles lost their internal regular porosity, as is evident from Fig. 2G and H. Particles of 12-SBA-15 sample surprisingly exhibit almost the same size and shape as the primary particles of parent SBA-15, but structural pores are much larger and irregular, reminiscent of worm-like structure. Even more significant is the change in 20-SBA-15 sample, where all particles are transformed and large needles and tabular bodies of vanadium oxide species are visible. It is in the line with character of XRD pattern of 20-SBA-15 sample, where no diffractions originated from hexagonal array of the mesopores are detected, but on the other hand diffraction pattern contains intense diffractions of V_2O_5 crystallites at 2θ between 15° and 35°. Structure of particles resembles phase separation phenomena relying on spinodal decomposition of the system [42, 43]. It means the silica is subjected to partial dissolution and gelation during the impregnation procedure. The reason is probably in high concentration of vanadium compound in the solution which is impregnated to reaching so high vanadium content in the resulting solid. It is well-know that vanadium is

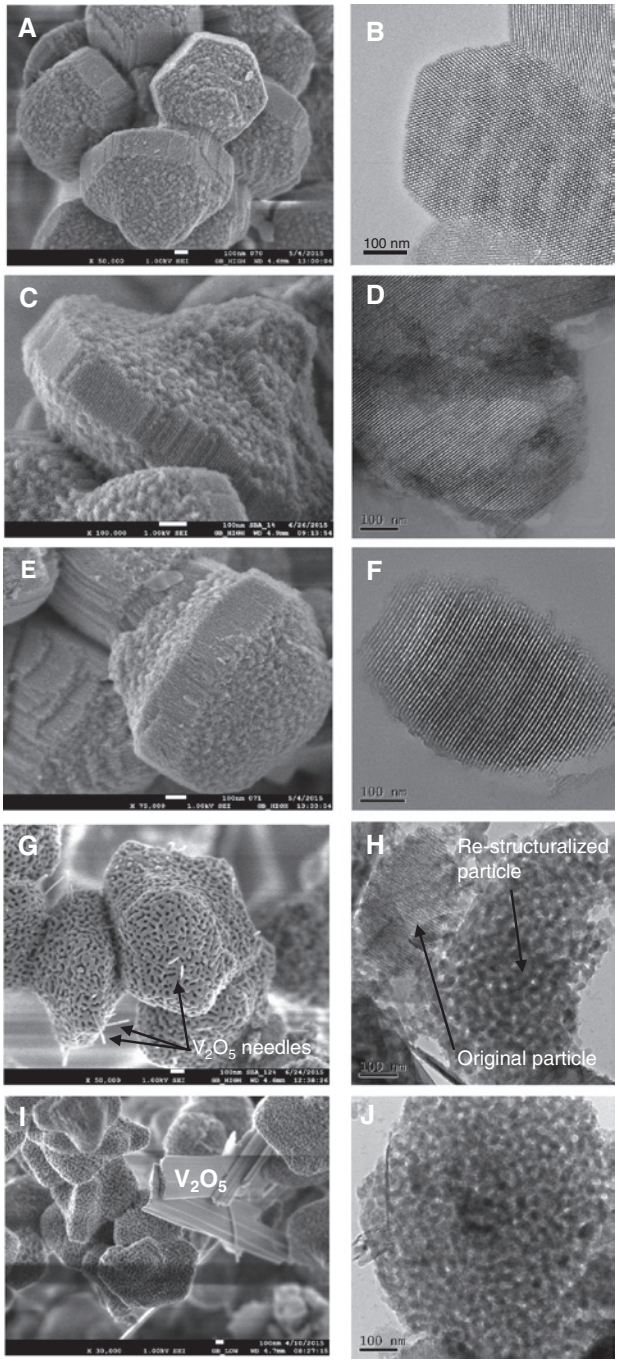

Fig. 2: SEM (left panel) and TEM (right panel) images of VOx-SBA-15 materials. A, B – parent SBA-15, C, D – 1-SBA-15, E, F – 9-SBA-15, G, H – 12-SBA-15, I, J – 20-SBA-15.

grievously detrimental to FCC zeolitic catalysts due to its corrosive behavior [44–48], thus it can be assumed that high concentrations of vanadium compounds in solution at elevated temperature will cause disruption of the silica wall. It is worth mentioning that such transformation of the silica was not observed in blank experiment, where pure SBA-15 silica was treated at the same conditions in the solvents without vanadium compounds and thus presence of some kind of vanadium species is crucial for this process.

N_2-physisorption isotherms and pore size distribution for all the VOx-SBA-15 samples are shown in Fig. 3A. The corresponding calculated textural parameters (specific surface area, total pore volume and maximum

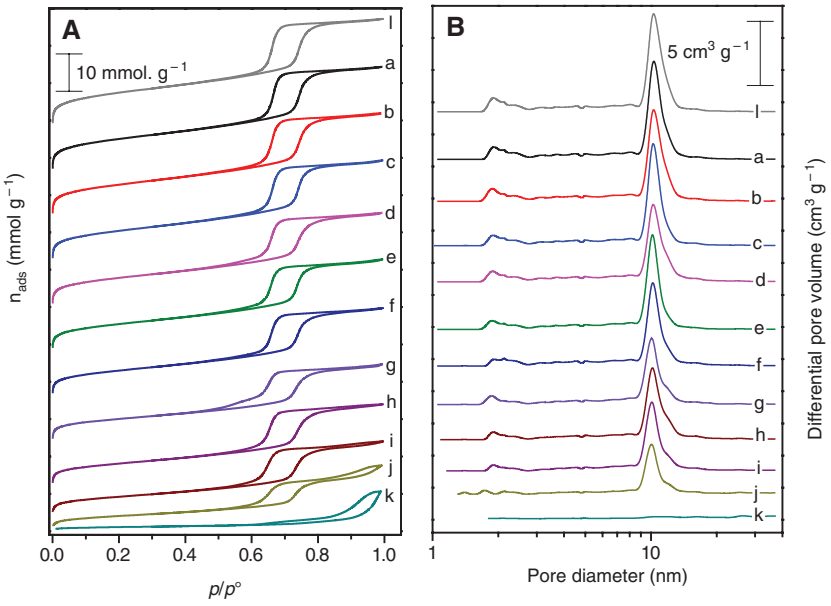

Fig. 3: Nitrogen adsorption/desorption isotherms at 77K for VOx-SBA-15 materials (A) and pore size distribution calculated by NL DFT approach (B). a: 1-SBA15, b: 2-SBA15, c: 3-SBA15, d: 4-SBA15, e: 5-SBA15, f: 6-SBA15, g: 7-SBA15, h: 8-SBA15, i: 9-SBA15, j: 12-SBA15, k: 20-SBA15, l: parent SBA15.

of the peak in PSD) for the parent SBA-15 and vanadium containing samples are summarized in the Table 1. Parent support exhibited adsorption isotherm typical for SBA-15 silicas, that is, isotherm of IV type with relatively narrow hysteresis loop of H1 type according to IUPAC classification [34]. The specific surface area was 762 $m^2 g^{-1}$ and pore volume was 0.971 $cm^3 g^{-1}$. Pore size distribution (PSD) curve exhibits narrow peak centered at 10.4 nm with half-width 1.6 nm (Fig. 3B). The N_2 adsorption/desorption isotherms for major the part of the prepared VO_x-SBA-15 samples resemble isotherm of parent SBA-15; they are of the IV type with H1 hysteresis loop (see Fig. 3A). The only exceptions are 12- and 20-SBA-15 samples with highest content of the vanadium (12 and 20 wt. %, resp.). Sample 12-SBA-15 exhibits secondary hysteresis loop at higher relative pressures indicating bimodal character of the pores with larger secondary pores. The most loaded sample, 20-SBA-15, exhibits even no original hysteresis loop at relative pressures from 0.6 to 0.7, but exhibits distinct capillary condensation at higher relative pressures characterized by hysteresis loop draw near to H3 type. This is clearly due to gelation and transformation of the silica during the vanadium impregnation leading to the disappearance of the original cylindrical pores and the creation of new, worm-like porous system as evidenced by SEM/TEM images (cf. Fig. 2). Similar changes in the character of hysteresis loops of adsorption isotherms recorded on SBA-15 silica materials modified by various guest phases introduced into silica by impregnation can be found in many published papers, but without deeper elucidation [8, 49–51].

Values of parameter C resulted from evaluation of adsorption data by BET equation are also listed in the Table 1. It can be seen that these values varies from 98 to 110 (with exception of 20-SBA-15 having value 120.5), but the change is not systematic. The parameter C reflects the adsorption enthalpy and surface heterogeneity or presence of different adsorption sites (like vanadium) should affect adsorption enthalpy and thus value of parameter C. However, no systematic change of C parameter is evident from data in the Table 1. In order to understand this observation, we measured and evaluated also adsorption isotherm of pure vanadium pentoxide sample. Interaction parameter C from BET equation for V_2O_5 was 115.5, thus very close to C parameter obtained for pure silica (101.4 for SBA-15 sample, and 99.7 for fumed silica sample). It means that interaction of nitrogen molecule with the surface of silica and vanadia surface is relatively similar and no significant changes of this parameter should be expected in VOx-SBA-15 samples.

It should also be noted that some samples exhibit tails at desorption branches of the isotherms. Such tail is most evident at the isotherm of 7-SBA-15 sample (see Fig. 3A, curve g). Widening and/or tail of the hysteresis

loop had already reported by Van Der Voort et al. [52, 53] and other authors [54, 55] and attributed to the formation of plugs or constrictions in the ordered channels of the SBA-15 silica. It means that some small vanadium oxide nanoparticles with size below 10 nm can be present in the channels and act as obstacle.

Pore size distribution functions for all investigated samples calculated by NL DFT methodology are shown in the Fig. 3B. PSD curves are characteristic by distinct peak at around 10 nm with small and poorly defined satellite at the border of the microporosity and mesoporosity (about 2 nm in diameter) which can be ascribed to the secondary microporosity of the SBA-15 silica wall as it was reported several times in the literature [56–58]. Textural characteristics (specific surface areas, pore volumes and maximum of the main peak in PSD) of the VOx-SBA-15 samples calculated from adsorption isotherms and pore size distribution curves depicted in the Fig. 3A and B, respectively, are summarized in the Table 1. It is clearly evident from the reported data that both specific surface area and pore volume decrease with increasing vanadium content in the sample. If we do not take into account the most loaded sample, we can say that S_{BET} and pore volume decrease proportionally to the vanadium content and the textural characteristic drops to approx. 40 % of original values for sample 12-SBA-15. On the other hand, the changes in mesopore size are negligible, the main peak position and shape is not altered by vanadium. Maximum of the peak varies between 10.4 and 10.0 nm.

To gain insight into nature of the vanadium species in the VOx-SBA-15 samples, a diffuse reflectance UV-vis and Raman spectroscopies were measured and will be briefly reported in the following text. The DR UV-vis spectra of the all prepared VO_X-SBA-15 materials are presented in the Figure 4A. These spectra contain several ligand to metal charge transfer absorption bands in the photon absorption energy ranging from 2.2 to approximately 5.7 eV. These bands can be ascribed to isolated (bands at 4.8 and 5.7 eV) and oligomeric tetrahedrally coordinated VO_X species (bands at *ca.* 4.1 and 4.8 eV) and to octahedrally coordinated polymerized VO_X species (bands at *ca.* 2.5 and 3.0 eV) according to the literature [38, 59–61]. It is clearly seen that for samples with less than 9 wt. % of vanadium, dispersed tetrahedrally coordinated species prevail on the surface of the SBA-15 materials and the exceeding of this limiting value causes start of the massive formation of the particles with the octahedral coordination structurally similar to the bulk V_2O_5. Spectra reveal that vanadium in the sample with lowest vanadium content is finely spread on the surface and predominantly isolated vanadyl

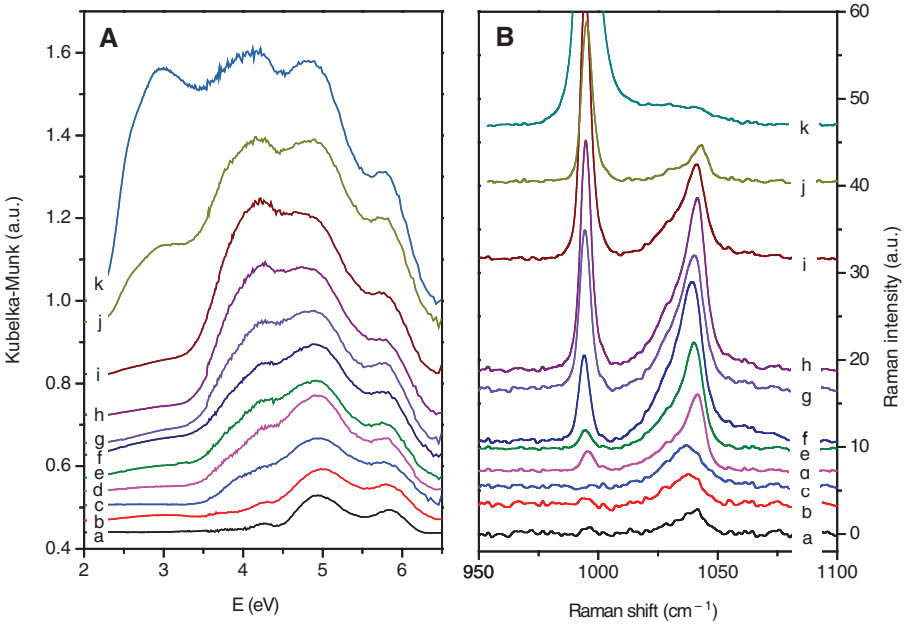

Fig. 4: Diffuse reflectance UV-vis spectra (A) and Raman spectra excited by 780 nm laser (B) of dehydrated VOx-SBA-15 samples under vacuum. a: 1-SBA15, b: 2-SBA15, c: 3-SBA15, d: 4-SBA15, e: 5-SBA15, f: 6-SBA15, g: 7-SBA15, h: 8-SBA15, i: 9-SBA15, j: 12-SBA15, k: 20-SBA15.

species are present in the sample. As vanadium content increases, the population of oligomeric vanadium species increases which is manifested by an increase of intensity of the band at around 4.1 eV and its shift to lower energies. Content of oxidic species in the low loaded samples is insignificant, as can be deduced from very low intensity of the spectra in the region of 2.5–3 eV. This is in line with Raman spectroscopy (see Fig. 4B). The Raman spectra of samples with content of vanadium up to 3 wt. % exhibit only one characteristic vibrational band at 1040 cm^{-1} assigned to the V=O vibration in isolated vanadyl species. Due to extremely high sensitivity of Raman spectroscopy to oxidic species, we can detect by Raman spectroscopy even traces of oxides. Very small peak at 995 cm^{-1} in the spectrum of 4-SBA-15 sample indicates the existence of some traces of V_2O_5 oxidic species. Intensity of the 995 cm^{-1} band increases for higher loadings of vanadium in the SBA-15 and it becomes dominant in the spectra of samples with the highest vanadium content in good agreement with intense band at 2.5 and 3 eV in DR UV-vis spectra (see Fig. 4A), presence of diffraction lines of crystalline vanadium pentoxide visible in the XRD patterns (Fig. 1B) and existence of needle-shaped or platy microcrystallites of V_2O_5 observed in the SEM images (Fig. 2).

Discussion

The above reported experimental data prove that set of VOx-SBA-15 samples covers wide range of systems from well-dispersed systems containing "atomically" dispersed vanadium as isolated vanadyl species to highly loaded systems containing mix of two separate phases of vanadium modified SBA-15 silica and V_2O_5 crystallites. In this context, it is understandable and not surprising that the textural characteristics of the systems examined will significantly change. Deeper inspection of experimental adsorption data reveals other details and new findings. It should be noted that data obtained on 12-SBA-15 and 20-SBA-15 samples exhibiting complete re-structuralization of the matrix and change in pore system character will not evaluated and commented in following text, due to ill-defined structure and absence of referent sample with the same textural characteristics without vanadium.

Even the low-loaded samples exhibit appreciable changes of specific surface area and pore volume, despite the fact that the vanadium in these systems is very finely dispersed. Partially it is caused by dilution of silica mass in the sample by vanadium, which contributes to the total specific surface area substantially less than silica. Nevertheless, data reported in the Table 1 show that introduction of even 1 wt.% of vanadium into SBA-15 silica causes a decrease in the surface area by 25 $m^2\ g^{-1}$ when compared with S_{BET} of pure SBA-15 silica (pure SBA-15 silica exhibits 762 $m^2\ g^{-1}$ while S_{BET} of 1-SBA-15 sample is 736 $m^2\ g^{-1}$). When we take into account, that content of SBA-15 silica in the 1-SBA-15 sample is 98.87 %, corrected S_{BET} of 1-SBA-15 sample will be 744 $m^2\ g^{-1}$, which is still significantly smaller than the surface area of parent SBA-15. This means that even if we take into account the dilution of the silica with vanadium and we will correct the values of the specific surface area and pore volume on the silica content in the samples, we will still observe the loss in both of these textural parameters. To gain insight into influence of vanadium presence on the surface, decrease of surface area corrected to the silica content in the sample expressed as difference of molar amount of N_2 molecules forming adsorption monolayer was related to the molar amount of vanadium atoms in the samples. Number of "missing" N_2 molecules in the adsorption monolayer per one vanadium atom anchored on the surface varies from one missing molecule of the adsorbed nitrogen per one anchored vanadium atom (or VO_X group) for the sample with 1 wt. % of vanadium to approximately 1.3 of the missing nitrogen molecules per 1 vanadium atom for samples with the vanadium content 6 wt. % (see Fig. 5). This value increases to 1.5–1.6 for samples with significant amount of oxide species, where some partial pore blocking or constrictions can be expected. It should be noted that sample 7-SBA-15 exhibiting distinct tailing of desorption branch of hysteresis loop and therefore larger extent of partial pore blocking, exhibits also higher value of "missing" N_2 molecules in the adsorption monolayer per one vanadium atom anchored on the surface compare with samples with 6 and 8 wt. % of vanadium.

The total pore volume determined from the adsorption isotherms at the equilibrium nitrogen relative pressure $x = 0.95$ also decreases as the concentration of the vanadium in the VO_x-SBA-15 materials increases.

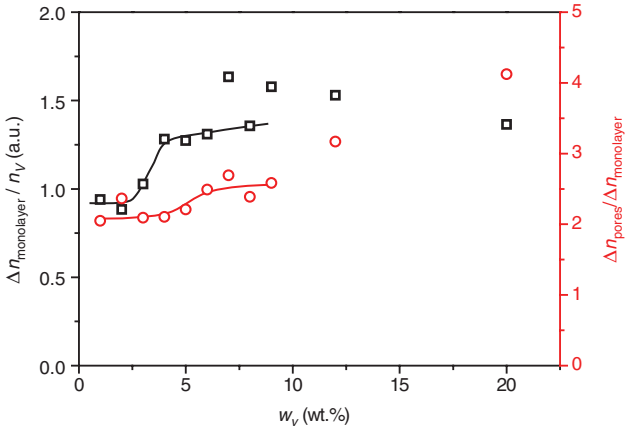

Fig. 5: Average number of "missing" nitrogen molecule in monolayer per vanadium atom (black squares) and statistical height of the multilayer N_2 adsorption affected by the presence of the anchored VO_x species (red circles) as a function of vanadium loading.

The amount of the nitrogen molecules, which are excluded from the condensation inside of the original SBA-15 pores by presence of VO_x particles, monotonously increases from value 2 molecules of nitrogen per one VO_x specie for the 1-SBA-15 sample up to approximately 6 molecules of the nitrogen per one VO_x specie for the 20-SBA-15 sample. If it can be adopted that the results of the BET fitting of data correspond to SBA-15 surface excluded from the first layer of the nitrogen adsorption then the ratio of excluded volume and the excluded surface corresponds to the statistical height of the multilayer N_2 adsorption affected by the presence of the anchored VO_x species (see Fig. 5). Obtained values of this height correspond to the two layers of adsorbed nitrogen molecules for samples with vanadium concentration lower than 5 wt. %. This corresponds to the formation of the isolated monomeric and oligomeric tetrahedrally coordinated VO_x species which represent at the most two-dimensional surface structures. Samples with the vanadium concentration between 5 and 9 wt. % exhibit the increasing of this value up to approximately 2.5 nitrogen layers. Such behavior can be ascribed to the starting of formation of the three-dimensional structures of anchored V_2O_5 like species which are evidenced by Raman and UV-vis spectroscopy (cf. Fig. 4). These findings led us to the conclusion, that surface area decrease observed ordinarily even for low loaded systems, where anchored species are too small to block pores and no destruction or alteration of the pores are detected by various characterization techniques, is caused by simply exclusion of certain space occupied by vanadyl complex from the adsorption of N_2 molecules as is outlined in the Fig. 6. This means that not all changes in the specific surface areas and the pore volumes are associated with the change of structure of the support.

In order to confirm the conclusions drawn from quantitative analysis of textural characteristics, we performed experiment with gentle flushing the vanadium species from sample 4-SBA-15 by ethanol. This sample exhibit quite large decrease in surface area (130 $m^2 g^{-1}$ compared to pure SBA-15) and contains negligible

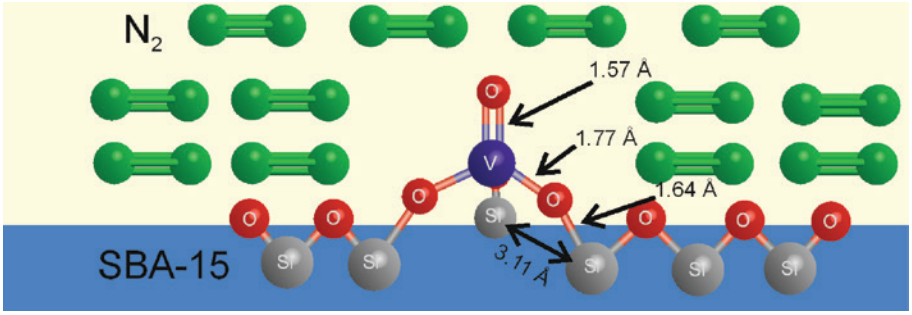

Fig. 6: Schematic representation of the spatial distribution of nitrogen molecules in close vicinity of surface vanadyl complex.

amount of oxidic species. Partial removing of vanadium from the surface of SBA-15 support (concentration of vanadium decrease from 4 wt. % to 0.8 wt. %) led to surface area increase by 50 $m^2 g^{-1}$ evidencing partial "restoration" of the pore volume and surface area.

Conclusion

Impregnation of SBA-15 by ethanolic solution of vanadyl precursor (vanadyl acetoacetonate) led to significant changes in the surface area and pore volume, as evidenced by evaluation of N_2 adsorption isotherms in accordance with observations of many authors in the literature. In the case of well-dispersed vanadium species, these changes cannot be explained by partial destruction of support or blocking of the mesopores, as frequently mentioned in the papers, but are caused by "dilution" of silica by presence of guest phase and exclusion small space occupied by surface vanadyl species from the adsorption of N_2 molecules. In addition to this effect, the presence of small oxide clusters in the mesopores, evidenced by DR UV-vis and Raman spectroscopies, can caused local narrowing the mesopores, which can contribute to the decrease of pore volume and surface area. The presence of narrower mesopores causes delayed evaporation of the liquid adsorptive leading to a lower desorption relative pressure and to tailing of the desorption branch of hysteresis loop, which can led to forced closure of the hysteresis loop at relative pressure 0.4–0.45 explained by tensile strength effect. Our results obtained on highly loaded SBA-15 samples presented here demonstrated that highly concentrated ethanolic solutions containing vanadium can attack silica matrix, partially dissolve it or form gel, which can led during drying and calcination of the material to the re-structuralization of the matrix and formation new, disordered porosity. Such materials exhibit quite different textural properties.

Acknowledgement: The authors thank the Czech Science Foundation for financial support under project No. 15-19780S. Lenka Zárybnická form UNICre Litvínov is kindly acknowledged for help with measurement of XRD patterns. In addition, we would like to thank Ivo Jakubec from Institute of Inorganic Chemistry of the Czech Academy of Sciences for performing TEM images and Veronika Podzemná from Center of Materials and Nanotechnology of University of Pardubice for SEM images.

References

[1] R. Martín-Aranda, J. Čejka. *Top. Catal.* **53**, 141 (2009).
[2] C. Perego, R. Millini. *Chem. Soc. Rev.* **42**, 3956 (2013).
[3] Ch. T. Kresge, W. J. Roth. *Chem. Soc. Rev.* **42**, 3663 (2013).
[4] J. Wang, L. Huang, R. Yang, Z. Zhang, J. Wu, Y. Gao, Q. Wang, D. O'Hareb, Z. Zhong. *Energy Environ. Sci.* **7**, 3478 (2014).
[5] Z. Zhang, D. L. Santangelo, G. ten Brink, B. J. Kooi, J. A. Moulijn, I. Melián-Cabrera. *Mater. Lett*. **131**, 186 (2014).
[6] J. Santamaria-Gonzalez, J. Luque-Zambrana, J. Merida-Robles, P. Maireles-Torres, E. Rodriguez-Castellon, A. Jimenez-Lopez. *Catal. Lett*. **68**, 67 (2000).
[7] S. A. Karakoulia, K. S. Triantafyllidis, A. A. Lemonidou. *Microporous Mesoporous Mat*. **110**, 157 (2008).
[8] T. Tsoncheva, L. Ivanova, R. Dimitrova, J. Rosenholm. *J. Colloid Interface Sci*. **321**, 342 (2008).
[9] R. Zhou, Y. Cao, S. R. Yan, J. F. Deng, Y. Y. Liao, B. F. Hong. *Catal. Lett*. **75**, 107 (2001).
[10] Y. M. Liu, Y. Cao, S. R. Yan, W. L. Dai, K. N. Fan. *Catal. Lett*. **88**, 61 (2003).
[11] R. Chlosta, G. Tzolova-Mueller, R. Schloegl, C. Hess. *Catal. Sci. Technol*. **1**, 1175 (2011).
[12] X. Chen, W. Zhao, F. Wang, J. Xu. *J. Nat. Gas Chem*. **21**, 481 (2012).
[13] C. Hess, J. D. Hoefelmeyer, T. D. Tilley. *J. Phys. Chem. B* **108**, 9703 (2004).
[14] I.-S. Park, S. Y. Choi, J. S. Ha, J. Khim. *Chem. Phys. Lett*. **444**, 161 (2007).
[15] P. Knotek, L. Capek, R. Bulanek, J. Adam. *Top. Catal.* **45**, 51 (2007).
[16] C. Hess, G. Tzolova-Mueller, R. Herbert. *J. Phys. Chem. C* **111**, 9471 (2007).
[17] W. Liu, S. Y. Lai, H. Dai, S. Wang, H. Sun, C. T. Au. *Catal. Lett*. **113**, 147 (2007).
[18] A. Held, J. Kowalska-Kus, K. Nowinska. *Catal. Commun*. **17**, 108 (2012).

[19] M. A. Smith, A. Zoelle, Y. Yang, R. M. Rioux, N. G. Hamilton, K. Arnakawa, P. K. Nielsen, A. Trunschke. *J. Catal*. **312**, 170 (2014).
[20] M. Piumetti, B. Bonelli, P. Massiani, S. Dzwigaj, I. Rossetti, S. Casale, M. Armandi, C. Thomas, E. Garrone. *Catal. Today* **179**, 140 (2012).
[21] M. A. Smith, R. F. Lobo. *Microporous Mesoporous Mat*. **131**, 204 (2010).
[22] E. Prouzet, C. Boissiere, S. S. Kim, T. J. Pinnavaia. *Microporous Mesoporous Mat*. **119**, 9 (2009).
[23] A. Dinse, B. Frank, C. Hess, D. Habel, R. Schomacker. *J. Mol. Catal. A-Chem*. **289**, 28 (2008).
[24] P. Kustrowski, L. Chmielarz, R. Dziembaj, P. Cool, E. F. Vansant. *J. Phys. Chem. B* **109**, 11552 (2005).
[25] Y.-F. Han, F. Chen, Z. Zhong, K. Ramesh, L. Chen, E. Widjaja. *J. Phys. Chem. B* **110**, 24450 (2006).
[26] Y. D. Bi, W. Zhang, H. Y. Xu, W. Z. Li. *Catal. Lett*. **119**, 126 (2007).
[27] B. M. Weckhuysen, D. E. Keller. *Catal. Today* **78**, 25 (2003).
[28] F. Cavani, N. Ballarini, A. Cericola. *Catal. Today* **127**, 113 (2007).
[29] R. Bulanek, A. Kaluzova, M. Setnicka, A. Zukal, P. Cicmanec, J. Mayerova. *Catal. Today* **179**, 149 (2012).
[30] J. W. Cahn, J. E. Hilliard. *J. Chem. Phys.* **28**, 258 (1958).
[31] A. Zukal, H. Siklova, J. Čejka. *Langmuir* **24**, 9837 (2008).
[32] R. Bulánek, P. Čičmanec, H. Sheng-Yang, P. Knotek, L. Čapek, M. Setnička. *Appl. Catal. A Gen*. **415– 416**, 29 (2012).
[33] S. Brunauer, P. H. Emmett, E. Teller. *J. Am. Chem. Soc.* **60**, 309 (1938).
[34] M. Thommes, K. Kaneko, A. V. Neimark, J. P. Olivier, F. Rodriguez-Reinoso, J. Rouquerol, K. S. W. Sing. *Pure Appl. Chem.* **87**, 1051 (2015).
[35] J. Rouquerol, P. Llewellyn, F. Rouquerol, *Stud. Surf. Sci. Catal*. **160**, 49 (2007).
[36] E. A. Ustinov, D. D. Do, M. Jaroniec, *Appl. Surf. Sci.* **252**, 1013 (2005).
[37] R. Bulánek, P. Čičmanec, M. Setnička. *Physics Procedia* **44**, 195 (2013).
[38] R. Bulánek, L. Čapek, M. Setnička, P. Čičmanec. *J. Phys. Chem. C* **115**, 12430 (2011).
[39] C. M. Yang, H. S. Sheu, K. J. Chao. *Adv. Funct. Mater.* **12**, 143 (2002).
[40] C. Yang, P. Liu, Y. Ho, C. Chiu, K. Chao. *Chem. Mat.* **15**, 275 (2003).
[41] L. Vradman, M. V. Landau, M. Herskowitz, V. Ezersky, M. Talianker, S. Nikitenko, Y. Koltypin, A. Gedanken. *J. Catal.* **213**, 163 (2003).
[42] A. Feinle, M. S. Elsaesser, N. Hüsing. *Chem. Soc. Rev.* **45**, 3377 (2016).
[43] J. Konishi, K. Fujita, K. Nakanishi, K. Hirao. *Chem. Mat.* **18**, 6069 (2006).
[44] C. A. Trujillo, U. N. Uribe, P. P. Knops-Gerrits, L. A. Oviedo. *J. Catal*. **168**, 1 (1997).
[45] X. Du, H. Zhang, G. Cao, L. Wang, Ch. Zhang, X. Gao. *Microporous Mesoporous Mat*. **206**, 17 (2015).
[46] U. J. Etim, B. Xu, Rooh Ullah, Z. Yan. *J. Colloid Interface Sci.* **463**, 188 (2016).
[47] E. Tangstad, A. Andersen, E. M. Myhrvold, T. Myrstad. *Appl. Catal. A-General*. **346**, 194 (2008).
[48] V. A. Tsiatouras, N. P. Evmiridis. *Ind. Eng. Chem. Res.* **42**, 1137 (2003).
[49] M. Piumetti, B. Bonelli, M. Armandi, L. Gaberova, S. Casale, P. Massiani, E. Garrone. *Microporous Mesoporous Mat*. **133**, 36 (2010).
[50] F. Gao, Y. Zhang, H. Wan, Y. Kong, X. Wu, L. Dong, B. Li, Y. Chen *Microporous Mesoporous Mat*. **110**, 508 (2008).
[51] L. Zhao, Y. Dong, X. Zhan, Y. Cheng, Y. Zhu, F. Yuan, H. Fu. *Catal. Lett.* **142**, 619 (2012).
[52] P. Van Der Voort, P. I. Ravikovitch, K. P. De Jong, A. V. Neimark, A. H. Janssen, M. Benjelloun, E. Van Bavel, P. Cool, B. M. Weckhuysen, E. F. Vansant. *Chem. Commun*. 1010 (2002).
[53] P. Van Der Voort P. I. Ravikovitch, K. P. De Jong M. Benjelloun, E. Van Bavel A. H. Janssen, A. V. Neimark, B. M. Weckhuysen, E. F. Vansant. *J. Phys. Chem. B* **106**, 5873 (2002).
[54] M. Kruk, M. Jaroniec, S. H. Joo, R. Ryoo. *J. Phys. Chem. B* **107**, 2205 (2003).
[55] J. P. Thielemann, F. Girgsdies, R. Schlögl, C. Hess. *Beilstein J. Nanotechnol*. **2**, 110 (2011).
[56] R. Ryoo, C. H. Ko, M. Kruk, V. Antochshuk, M. Jaroniec. *J. Phys. Chem. B* **104**, 11465 (2000).
[57] M. Kruk, M. Jaroniec, C. H. Ko, R. Ryoo, *Chem. Mat.* **12**, 1961 (2000).
[58] A. Galarneau, H. Cambon, F. Di Renzo, R. Ryoo, M. Choib, F. Fajula. *New J. Chem.* **27**, 73 (2003).
[59] X. Gao, S. R. Bare, B. M. Weckhuysen, I. E. Wachs. *J. Phys. Chem. B*. **102**, 10842 (1998).
[60] I. E. Wachs, C. A. Roberts. *Chem. Soc. Rev.* **39**, 5002 (2010).
[61] Z. L. Wu, S. Dai, S. H. Overbury. *J. Phys. Chem. C,* **114**, 412 (2010).